Robotica (2014) volume 32, pp. 501–513. © Cambridge University Press 2013
doi:10.1017/S0263574713000817

Effects of substituting anthropometric joints with revolute joints in humanoid robots and robotic hands: a case study

Mehdi Mousavi†,‡*, Aurelio Somà† and Francesco Pescarmona‡

†*Department of Mechanical Engineering, Politecnico di Torino, Corso Duca degli Abruzzi 24, 10129 Torino, Italy*
‡*Center for Space Human Robotics at PoliTo, Istituto Italiano di Tecnologia, C.so Trento 21, 10129 Torino, Italy*

(Accepted July 24, 2013. First published online: August 22, 2013)

SUMMARY
In the human body there are many joints whose functions are very similar to revolute joints. To avoid the complexity of these joints, they are usually substituted by revolute joints in many humanoid robots. Revolute joints have purely rotational motion along their fixed axis, while real joints in the human body have Instantaneous Rotational Axis (IRA) due to their configuration. Substitution of this kind of human joints with revolute (hinge) joints in robots changes the kinematics of joints. Knowing the exact characteristics of the moving axis of rotation in human joints is a prerequisite for the kinematic study of a joint. Here the main geometrical difference between these kinds of joints in humans and their simplified (hinge-like) models in robots is described. Then, as a case study, the mechanism of the three joints of the index finger are compared with their hinge-like model using a multi-body code to understand when revolute joints can be substituted for anthropometric joints in hand exoskeletons and robotic hands. Furthermore, the position of IRA and its distance from the center of the condyle of the joint are presented. The concept and the results can be extended for other fingers and all similar joints, and can be used in humanoid robots, hand exoskeletons and robotic hands.

KEYWORDS: Humanoid robots; Robotic hands; Hand exoskeletons; Human joints; Finger biomechanical model; Finger kinematics, Distal interphalangeal; Proximal interphalangeal; Metacarpophalangeal.

Nomenclature

B: The base (concave) side of the phalanx
D: Distance of the fingertip position in two models
H: The head (condyle) side of the phalanx
L_P: The length of the proximal phalanx
L_M: The length of the middle phalanx
L_D: The length of the distal phalanx
M_H: The center of curvature of the head (condyle) side of the phalanx
R: The distance between M_H and M_B
r_H: The radius of curvature of the head (condyle) side of the phalanx
r_B: The radius of curvature of the base (concave) side of the phalanx
W_H: The width of the head (condyle) side of the phalanx
W_B: The width of the base (concave) side of the phalanx
α: The resultant angle of rotation of each bone after rotation

* Corresponding author. E-mail: mehdi.mousavi@polito.it

https://doi.org/10.1017/S0263574713000817 Published online by Cambridge University Press

α_H: Angle of rotation around M_H
α_B: Angle of rotation around M_B

1. Introduction

There are many joints in the human skeleton. Some of them, such as the finger distal interphalangeal (DIP) joint and the proximal interphalangeal (PIP) joint, have just one degree of freedom, and their function is very similar to revolute (hinge) joints. Others, such as the finger metacarpophalangeal (MCP) joint, the elbow, knee and ankle joints, which have more than one degree of freedom, can also be considered as revolute joints if just one of their degrees of freedom is desired.

Many researchers have already studied the kinematics of human joints, and many humanoid robots and robotic hands have already been developed, but in most of these the mechanism of the human joints and, consequently, the robot joints has been considered as a series of links connected together with normal revolute joints. For example, different kinematic models have been presented for human finger joints in which the DIP, PIP and MCP joints of the fingers are considered as revolute joints that connect the finger phalanges together.[1–3] Based on this approach, different mechanisms have been proposed in literature.[4–6] In some other papers, the elbow, the knee and other similar joints of the body are substituted with revolute joints, and their simplified models have been presented.[7–9] These simplified kinematic models have been used by researchers to develop hand exoskeletons[10–14] and humanoid robots.[15–17] Here this model of joints, which has purely rotational motion along the fixed joint axes, is called the hinge-like model of the joint. This approach is widely used in robotic hands, hand exoskeletons and humanoid robots to avoid the complexity of the two articulating surfaces of human joints.

However, the results of non-invasive tests based on surface marker measurement to determine the knee and finger joints' axes of rotation showed that the marker trajectories do not follow a pure rotation around a fixed axis.[18–20] Therefore, an optimization technique is usually used in such investigations to find the best fitted point (point instead of axis when projected on a plane) among the acquired cloud data for the center of rotation (COR), and this proves that the COR of each phalanx is a moving point.[21–23] Therefore, using a revolute joint, which has a fixed axis of rotation instead of an anthropometric joint in robots, changes the kinematics of the joint.

On the other hand, if a pulling force is applied along each extended articulation of the human body, for example, extended fingers or extended knees, a minor axial movement occurs. This happens due to the characteristics of human joints in which the two main segments of the joints are not rigidly connected together like in a normal hinge joint but with a series of stretchable ligaments that encompass the two adjacent bones. This behavior cannot be simulated with the traditional hinge-like model of the joints in robots. Therefore, an improved model, which is capable of taking these issues into account, is necessary in robot design if a reliable model of human joints is desired.

From another point of view, robots usually use a closed loop control system to mimic human movements. The closed loop control helps the system to compensate errors coming from differences between kinematics of human joints and robot joints. However, if an open loop control is desired, the kinematic model of the joints of the robot has to be as similar as possible to human joints in order to achieve an identical configuration. This confirms the importance of a precise model of human joints.

In order to develop such a model, differences in geometry, which are the main reasons for kinematic differences between the anthropometric model and the hinge-like model of human joints, is explained. Since it is difficult to study here the geometry of all types of human joints, the study of the finger joints and all other similar joints, such as the elbow and knee joints, is the focus of this paper.

Then, to provide a standard that describes when it is acceptable to consider this kind of joints as a hinge, a case study of the human index finger is presented. Moreover, the effects of using the proposed model on the kinematics of the finger and on the fingertip position are investigated.

Therefore, the geometry of each finger phalanx is created in SolidWorks and imported into a multi-body environment (Adams/View). Two models of the index finger, one based on the hinge-like approach and the other based on the incongruity of the articulating surface curvatures, are created. Finally, the results of using these two different models are compared based on a number of simulations.

Although the human index finger is chosen as a case study, the concept can be generalized for other fingers and all similar human joints, such as knee joints, and the results of the present work should be considered in the design of humanoid robots, hand exoskeletons and robotic hands.

https://doi.org/10.1017/S0263574713000817 Published online by Cambridge University Press

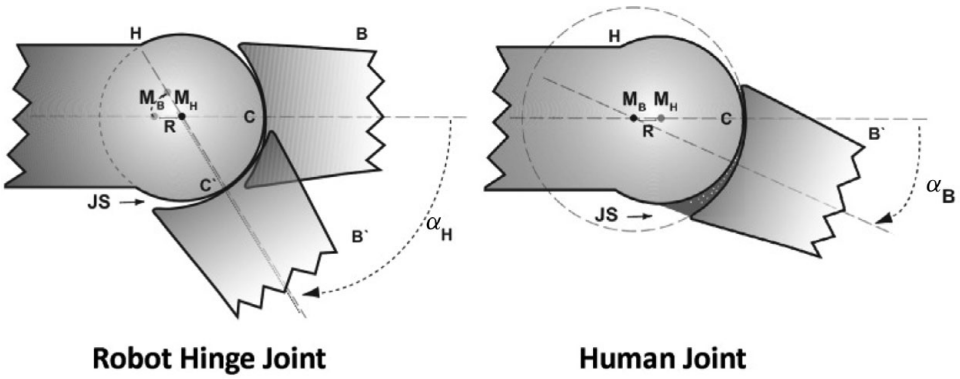


Fig. 1. Comparison of human joint and robot hinge joint.[24]

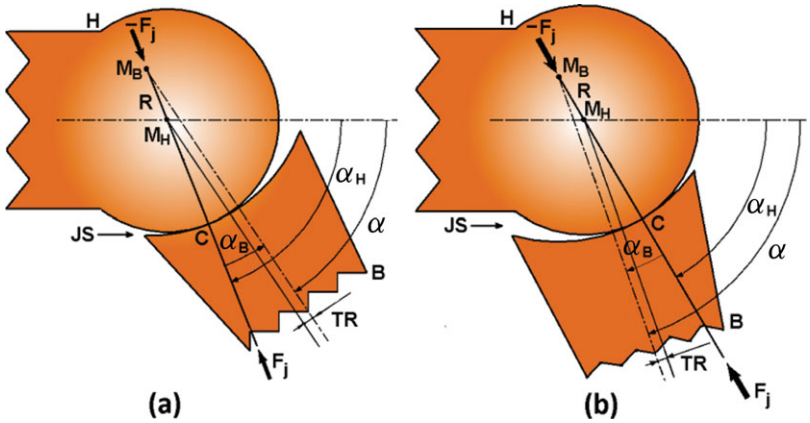


Fig. 2. (Colour online) Fundamental geometrical parameters of human joints: (a) when $\alpha_H > \alpha$ and (b) when $\alpha_H < \alpha$. Consider the position of the contact point C and Joint Space (JS).[24]

2. Method

2.1. Fundamental geometrical parameters of human joints

It can be inferred from Fig. 1 that the main reason for the difference between the kinematics of a human joint and a robot hinge joint is the difference in their shapes and their working mechanisms. In a hinge joint, two parts of the joint are connected together through a round bar (pin) and a pure rotation occurs around a fixed axis. Therefore, the joint space (JS) remains unchanged during flexion and extension of the joint. However, in human joints, the condyle of one bone is placed over the concave base of the other bone and due to the difference of curvature of the two contacting surfaces, a mixture of rotation and sliding occurs. Therefore, JS changes during flexion and extension (Fig. 2).

The assumption that some human joints work like hinge joints implies that the two articulating surfaces must show congruity of their curvatures,[24] and this contradicts the anatomical studies that prove the incongruity of the surface curvature of these joints.[25–28]

In Fig. 2 a kinematic model of human joints in flexion is explained by some fundamental geometrical parameters. According to this kinematic model, a flexion in the joint is composed of two fundamental rotations that take place simultaneously: (1) α_H around M_H, and (2) α_B around M_B. This theory is proposed by Dumont[24] for the PIP joint, but is also true for the DIP, MCP and other similar human joints. By using this kinematic model, which is closer to reality than the hinge-like model, the resultant position of each bone after rotation can be considered as being composed of a rotation α around the condyle center (M_H) plus an additional translation, TR (Fig. 2).

Since there is no data regarding the range of the above-mentioned parameters and their functional effects in literature, the influence of these parameters is not clear and the effects arising from substituting this anthropometric model with a hinge-like model in robots are unknown.

https://doi.org/10.1017/S0263574713000817 Published online by Cambridge University Press

As mentioned before, in order to acquire this information and to understand when anthropometric joints can be substituted with revolute joints in robots, a case study for the three joints of the index finger is performed using a multi-body code. General description and analytical equations of the multi-body approach used by the authors can be found in refs [29, 30].

2.2. Creating the model

In order to be very precise regarding the dimensions of the finger phalanges and the shape of their articulating surfaces, X-ray radiography or laser scanning technology can be used. However, the results will be valid only for the specific case that is being measured. Therefore, to increase the generalizability of the research, it is decided to extract the dimensions of the finger phalanges and the shape of the articulating surfaces from previously published papers. In these papers, different methods of measurement have been used, such as X-ray radiography, laser scanning, or casting of hands from cadavers.

With some simplifications, at least six major parameters are required to design each joint of the index finger: the lengths of the two adjacent phalanges, the radii of their contacting surfaces and their widths.

As mentioned above, here the lengths of the proximal, middle and distal phalanges (L_P, L_M and L_D), the radii of curvature and the widths of both sides (head and base) of each one (r_H, r_B, W_H and W_B) are extracted based on the data proposed in literature. As far as possible, the correctness of each chosen number has been checked with other papers.

In a study done by Gibson[31] in 2005, a reverse engineering-based method was used to measure the dimensions of finger bones. Altogether, 79 finger joint bone specimens from 10 hands of nine cadavers were scanned by laser, eight of which were left-hand joints and the other two were right-hand joints. The results of this clinical practice for L_P of the index fingers are 40, 42, 44 and 46 mm with frequencies of 3, 4, 2 and 1 respectively. The average of these results is 42.2 mm.

In another study,[32] the average lengths of finger phalanges have been given as $L_P = 39.78 \pm 4.94$, $L_M = 22.38 \pm 2.51$ and $L_D = 15.82 \pm 2.26$. These data were derived from the X-ray images of right and left hands of 19- to 78-year-old 66 adults without any bone pathology or deformities. These numbers are 39.95 ± 3.55, 24.00 ± 2.2 and 17.65 ± 1.75 for the index finger of 39 subjects (23 males and 16 females) in ref. [33]. Ash and Unsworth[28] also dissected 83 joints from 21 hands of 55- to 81-year-old 11 cadavers (seven males and four females). In their study, L_P ranged from 29 to 52 mm (mean 43.20 mm) and L_M ranged from 16 to 35 mm (mean 27.12 mm). In our model, L_P, L_M and L_D are 42.2, 24.6 and 17 mm respectively, which are within the range of the results of all the four above-mentioned studies.

Moreover, according to the works of Kenesi,[34] the head of the proximal phalanx averages about 11.5 mm in width (W_{PPH}) and the base of the middle phalanx measures 12.6 mm in width (W_{MPB}).

For W_{PPH}, Buryanov and Kotiuk[32] published the measured numbers of 11, 12 and 13 mm with repetitions of 4, 4 and 2 mm respectively. The average of these 10 results is 11.8 mm. It can be seen that the calculated number of 11.8 mm is very close to what Kenesi[34] proposed, i.e. 11.5 mm. Here 11.8 mm is chosen as W_{PPH}.

Relationships between the geometrical parameters of the bones along with their correlation coefficients have been proposed by some formulas in ref. [31]. To calculate the width of the proximal phalanx on the base side (W_{PPB}), since the correlation coefficient between W_{PPH} and W_{PPB} is high (84.4%), the formula that relates these two parameters ($W_{PPH} = 0.741W_{PPB} - 0.733$) is used. By using $W_{PPH} = 11.8$ mm in this formula, W_{PPB} will be 16.91 mm.

For the width of the middle phalanx on the base side (W_{MPB}), since the correlation coefficient between W_{MPB} and W_{PPH} is the highest (91.6%), the following formula is used: $W_{MPB} = 1.272W_{PPH} - 0.924$. Therefore, by substituting $W_{PPH} = 11.8$ mm in this formula, W_{MPB} will be 14.1 mm, which is 1.5 mm more than 12.6 mm, the value proposed in ref. [34]. In this paper, 14.1 mm is chosen as W_{MPB}.

In 2008, by casting the proximal, middle and distal phalanges of the hands obtained from cadavers, Dumont[26] proposed the mean values of the radii of curvature for the articulating surfaces of the MCP, PIP and DIP joints. The radii and centers of joint surfaces were measured in 40 PIP joints (without macroscopic signs of arthrosis, equally distributed in right and left hands). The results are shown in Table I.

https://doi.org/10.1017/S0263574713000817 Published online by Cambridge University Press

Table I. The radii of curvature of the proximal and distal ends of the MCP, PIP and DIP joints for all fingers according to Dumont *et al.*[26].

Joints radii for all fingers (mm)	MCP	PIP	DIP
Radii of concave (distal end of the articulating surface) (r_B)	10	5.4	3.7
Radii of condyle (proximal end of the articulating surface) (r_H)	6	4.1	2.8
Percentage of difference	67	30	32
r_B/r_H	**1.670**	1.30	**1.320**

Table II. The radii of curvature of the proximal and distal ends of the PIP joint for the index finger according to Dumont *et al*.[24].

Joints radii for all fingers (mm)	MCP	PIP	DIP
Radii of concave (distal end of the articulating surface) (r_B)	–	5.68	–
Radii of condyle (proximal end of the articulating surface) (r_H)	–	4.28	–
Percentage of difference	–	32.7	–
r_B/r_H	–	**1.327**	–

In another paper by Dumont,[24] the results of the same study, but only for the PIP joints of the fingers, were presented. Table II shows these results. The percentage of incongruity for the PIP joint of the index finger is 32.7% according to these data.

Since only the model of the index finger is simulated here, the data presented for the index finger in Table II allow more accurate figures for the PIP joint to be calculated. However, for the MCP and DIP joints the data from Table I are used in our model.

It should be emphasized that all the geometrical parameters used in our simulations are related to specific persons and are subject to change for other people. However, the mean values presented in all previously mentioned papers were used in order to be more generally applicable.

In order to have more comprehensive results, in the first step, three simulations of the PIP joint for 10% more and 10% less than the average incongruity (32.7%) are performed. In other words, in three different simulations of the PIP joint, the r_B/r_H ratios are 1.227, 1.327 and 1.427.

In the second step, to understand the effects of substituting anthropometric/human joints with revolute joints on the position of the fingertip, two models of the finger are compared. One method presents an incongruity of the joints surface curvature with the r_B/r_H ratios of 1.670, 1.327 and 1.320 for the MCP, PIP and DIP joints respectively, while the other has hinge-like joints.

2.3. Multi-body model characteristics

In order to model the human finger phalanges in Adams/View package, after creating a precise surface geometry for each phalanx, the contact parameters between adjacent phalanges have to be defined. In Adams/View, contacts are grouped into two categories: two-dimensional contacts, which include the interaction between planar geometric elements, and three-dimensional contacts, which include the interaction between solid geometries.[35] Since a three-dimensional analysis is performed, a solid to solid contact is selected. In addition, the contact has two built-in functions in Adams/View: *impact* and *restitution*. In the impact function, the forces of the contact are modeled as spring-dampers with adjustable stiffness and maximum damping. Moreover, the spring force can also be modified by adjusting a force exponent. In the restitution function, a constant penalty force is applied in the direction opposite to motion. In addition, a coefficient of restitution determines the energy loss of the contact.[36]

If the restitution method is desired, the coefficient of restitution data is required from material references or physical testing. These data are unknown in this study. In addition, the impact method is faster and numerically smoother than the restitution method and provides a better control of the contact behavior, with adjustable distance to maximal damping and force exponent.[35,36] Therefore, the impact method is chosen in this study. Four parameters have to be set in Adams/View package for calculating normal forces when the impact method is chosen: stiffness, force exponent, damping and penetration depth.

https://doi.org/10.1017/S0263574713000817 Published online by Cambridge University Press

The stiffness parameter depends not only on material properties but also on the geometry of the objects in contact. In general, higher stiffness means that the two bodies are more rigid or hard. There is no handbook for choosing the value for the stiffness. The best option is to do multiple simulations in Adams with different values of stiffness to determine the optimal value, the value at which no fluctuation in the contact forces exists or the Adams contact behavior resembles the real-world contact behavior.[37,38] Using this approach, the stiffness value is adjusted to 1.5 (N/mm), at which the contact forces became constant.

Another parameter that has to be set is force exponent. Adams/Solver models normal force as a nonlinear spring-damper. If the damping penetration is the instantaneous penetration between the contacting geometry, Adams/Solver calculates the contribution of material stiffness to the instantaneous normal forces. Force exponent should normally be set to 1.5 or higher based on refs [35, 39].

Damping is the third parameter that has to be set following the choice of the impact method, a value to define the damping properties of the contacting material. Based on refs [35, 39], the damping coefficient is about 1% of the stiffness coefficient.

The last parameter to be defined is penetration depth, the value at which Adams/Solver applies full damping. It uses a cubic step function to increase the damping coefficient from zero, at zero penetration, to full damping when the penetration reaches the specified penetration depth. A reasonable value for this parameter is 0.01 mm according to refs [35, 39].

Based on the above-mentioned information, in the model with the incongruity of its joint surfaces, a solid to solid contact between the two adjacent phalanges of each joint is defined in Adams/View package with the following characteristics: normal force: impact, stiffness = 1.5 (N/mm), force exponent = 2.2, damping = 1.5×10^{-2} (N s/mm), penetration depth = 0.01 (mm) and friction force: none. The main spring connects the centerlines of each of the two bodies to keep them in contact and prevent their separation. As the analysis is just for flexion, a small force is applied on the lower surface of each phalanx to simulate tendon forces in flexion. The direction of this force is similar to that of tendons, and it has to be emphasized that with a small change in the force direction, the results do not change significantly.

A schematic view of the finger designed in Adams is shown in Fig. 3. A 3D model of the finger and details of the PIP and DIP joints can be seen in this figure.

3. Results

3.1. Geometrical parameters of two models

In the first step, the most important geometrical parameters of the model were recorded one by one for three performed simulations of the PIP joint with the r_B/r_H ratios of 1.227, 1,327 and 1.427. The results can be seen in Table III. The data show the values of rotation around two centers of curvature, α_H around M_H and α_B around M_B, along with TR for each angle (α).

The positions of IRA are plotted in the *x*–*y* coordinate plane in Fig. 4, in which the reference point (0,0) is located at M_H. As can be seen in this figure, the position of IRA is not a fixed point at M_H but moves during time. Moreover, the positions of IRA are mostly located in quadrants II and IV of the Cartesian coordinate system.

Figure 5 shows the distance between IRA and M_H. It can be seen that this distance oscillates between 0 and its maximum values for all three ratios of r_B/r_H. While it reaches zero (or near zero) several times, it reaches R (or near R) just a few times. This means that a pure rotation around M_H is much more than a pure rotation around M_B. This is in agreement with the geometric evaluations performed by Dumont[24] and will be discussed later.

Figure 6 shows the values of TR for each α. TR = 0 shows the angle at which the contact point of the two segments of the PIP joint (point C) passes the centerline of the middle phalanx. This angle is 70.78°, 64.2° and 73.39° for the r_B/r_H ratios of 1.227, 1.327 and 1.427 respectively.

As expected, point C always moves on a curve with the radius of the condyle of the proximal phalanx. Contrary to a hinge-like joint, this movement does not have a smooth trend. In Fig. 7 the position of point C for the model with the r_B/r_H ratio of 1.327 is shown with a solid line and for the hinge-like model with a dashed line. At the beginning of the motion, point C moves downward

https://doi.org/10.1017/S0263574713000817 Published online by Cambridge University Press

Table III. Values of α_H, α_B and TR for three ratios of r_B/r_H (1.227, 1,327 and 1.427) for the PIP joint.

	$r_B/r_H = 1.227$			$r_B/r_H = 1.327$			$r_B/r_H = 1.427$		
α°	α_H°	α_B°	TR (mm)	α_H°	α_B°	TR (mm)	α_H°	α_B°	TR (mm)
0	0.0	0.0	0.000	0.0	0.0	0.000	0.0	0.0	0.000
10	22.9	−12.9	0.233	20.9	−10.9	0.268	21.4	−11.4	0.341
20	31.0	−11.0	0.202	32.1	−12.1	0.300	33.8	−13.8	0.416
30	40.8	−10.8	0.198	40.3	−10.3	0.255	42.4	−12.4	0.379
40	49.9	−9.9	0.181	50.3	−10.3	0.253	51.4	−11.4	0.347
50	60.1	−10.1	0.188	57.6	−7.6	0.188	61.6	−11.6	0.352
60	66.2	−6.2	0.114	63.9	−3.9	0.095	71.0	−11.0	0.334
70	70.7	−0.7	0.012	61.2	8.8	0.214	74.6	−4.6	0.134
80	66.1	13.9	0.250	63.4	16.6	0.395	67.2	12.8	0.377
90	70.8	19.2	0.342	74.8	15.2	0.364	72.2	17.8	0.512
100	82.9	17.1	0.306	80.8	19.2	0.455	86.1	13.9	0.406
110	86.3	23.7	0.415	88.0	22.0	0.505	91.4	18.6	0.537

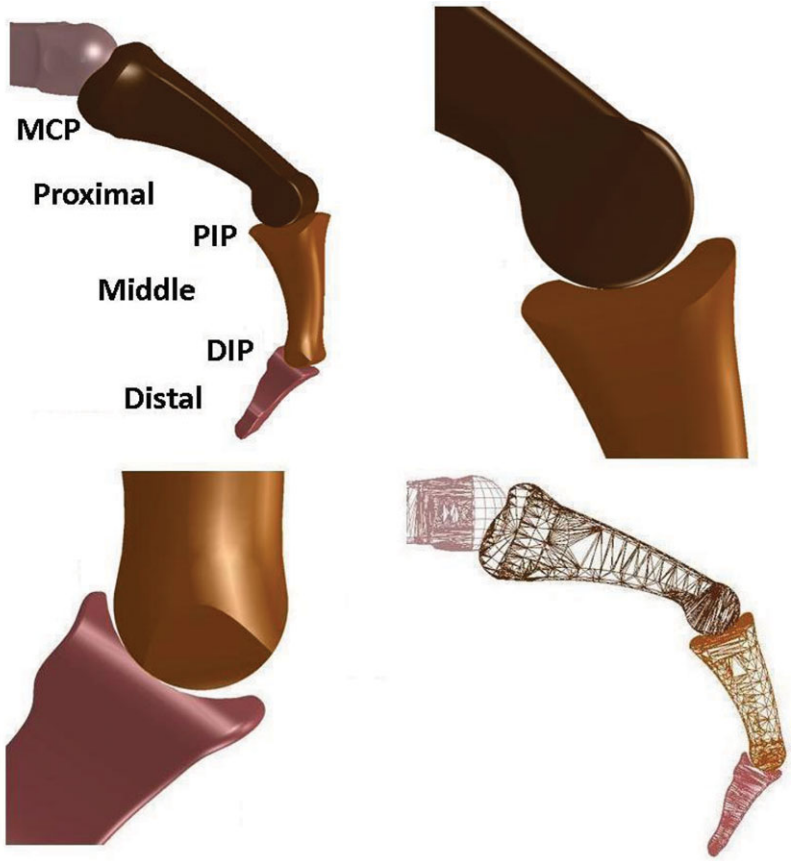


Fig. 3. (Colour online) Schematic view of the designed finger in Adams (a 3D model of the finger and details of the PIP and DIP joints).

very fast. It shows that a more significant rotation has occurred around M_B than around M_H. Then the rotation around M_H increases and this rotation is dominant until α is around 60° .

During this period, point C moves downward almost at a fixed rate. At $\alpha = 64.2^\circ$, point C passes the centerline of the middle phalanx and the two curves cross each other. After $\alpha = 64.2^\circ$, the rotation around M_B starts again to become more prominent so that point C starts to rise. Around $\alpha = 73^\circ$ until the end of flexion, the prominent rotation is once again around M_H and point C moves downward

https://doi.org/10.1017/S0263574713000817 Published online by Cambridge University Press

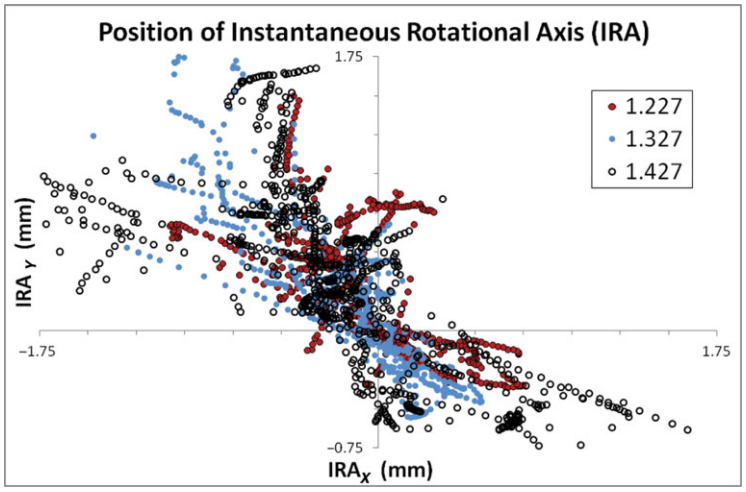


Fig. 4. (Colour online) Positions of IRA in the x–y-coordinate plane for r_B/r_H of 1.227, 1.327 and 1.427. The location of IRA is not a fixed point at M_H (0, 0). It moves during time mostly within 1.5 to 2 mm around M_H.

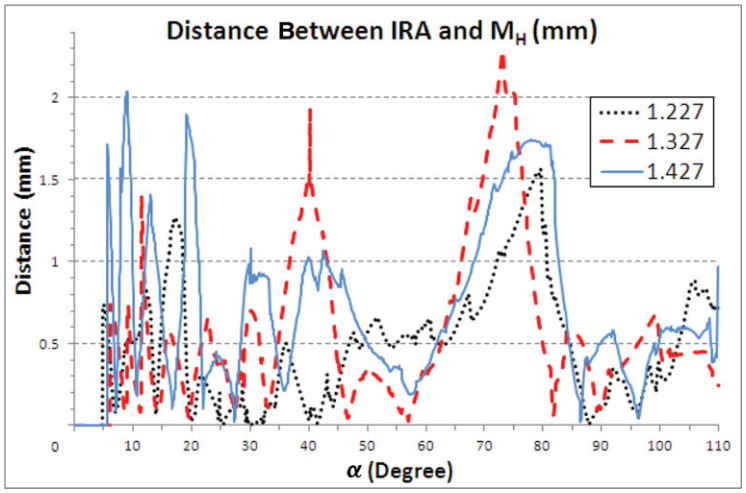


Fig. 5. (Colour online) Distance between IRA and M_H for each α for r_B/r_H of 1.227, 1.327 and 1.427.

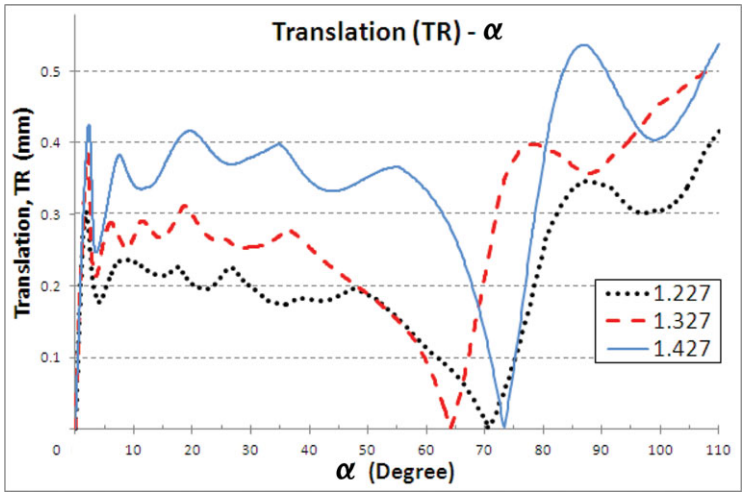


Fig. 6. (Colour online) Values of translation (TR) for each α for r_B/r_H of 1.227, 1.327 and 1.427.

https://doi.org/10.1017/S0263574713000817 Published online by Cambridge University Press

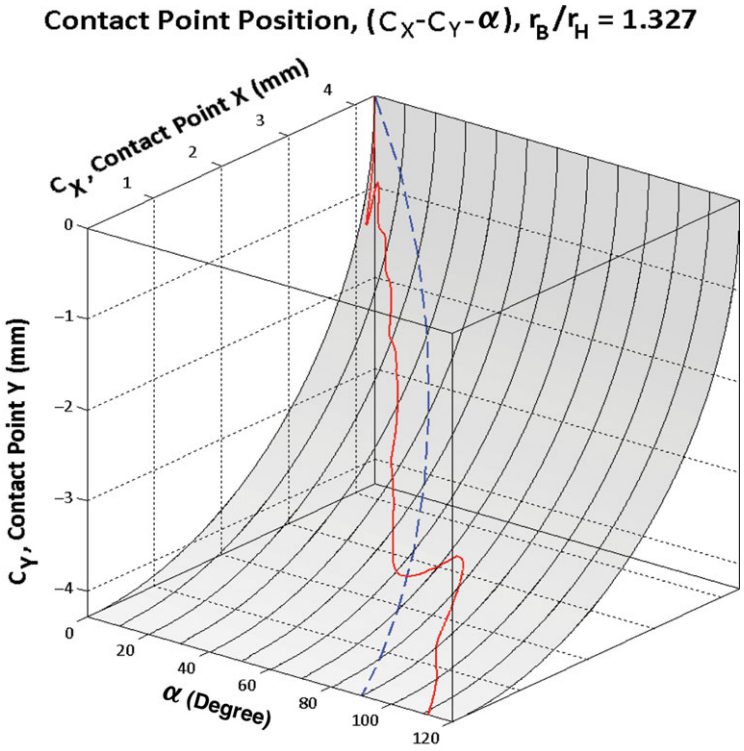


Fig. 7. (Colour online) Comparison of the motion route of the contact point C, the model with incongruity of surface curvature (solid line) and the traditional hinge-like model (dashed line).

at almost fixed rate. In the hinge-like model, point C reaches $x = 0$ (exactly under M_H) at $\alpha = 90^\circ$, whereas by considering incongruity, it reaches the same point at $\alpha = 111.28^\circ$.

This description can be illustrated by some other important parameters, α, α_H and α_B, which are plotted in Fig. 8 for the r_B/r_H ratio of 1.327. While α_H can be used to explain the position of contact point C on the condyle of the proximal phalanx, α_B shows the position of C on the curvature of the proximal end of the middle phalanx. It can be seen in Fig. 8 that after the first 5°, except for α from 60° to 73°, α_H has almost the same rate of increase. It means that the contact point C tends to move downward on the condyle of the proximal phalanx with almost a fixed rate. However, α_B remains almost fixed for α between 5° and 50°. This means that the position of point C remains almost fixed on the surface of the proximal end of the middle phalanx while it moves downward on the condyle of the proximal phalanx. Around 50°, point C starts to move on the base surface of the middle phalanx and passes its centerline. After α is about 75°, α_H again remains almost unchanged and point C remains fixed on the surface of the proximal end of the middle phalanx while it moves on the condyle of the proximal phalanx. These explanations are also valid for other r_B/r_H ratios. This behavior is plotted step by step in Fig. 9. The two highlighted configurations in this figure show the moment at which point C moves from the left side to the right side of the phalanx centerline. For the r_B/r_H ratio of 1.327 this occurs at $\alpha = 64.2^\circ$ at which $\alpha_B = 0, \alpha = \alpha_H$ (Fig. 8) and TR = 0 (Fig. 6).

3.2. Difference of the fingertip position in two models

In the second step, another simulation with all three phalanges of the index finger is performed to understand the functional effects of the model presented and that of traditional hinge-like model. Then the position of the fingertip in the two models is compared.

Since the soft tissue at the tip of the index finger is presented as 3.84 ± 0.59 mm,[33] this value is also considered in the calculations. First, the MCP and PIP joints are fixed and only the DIP joint is allowed to rotate. In this situation, for different angles of the DIP joint, the fingertip position is measured in two models and the distance (D) between these two points is calculated. Then the same analysis is performed for PIP and MCP joints.

https://doi.org/10.1017/S0263574713000817 Published online by Cambridge University Press

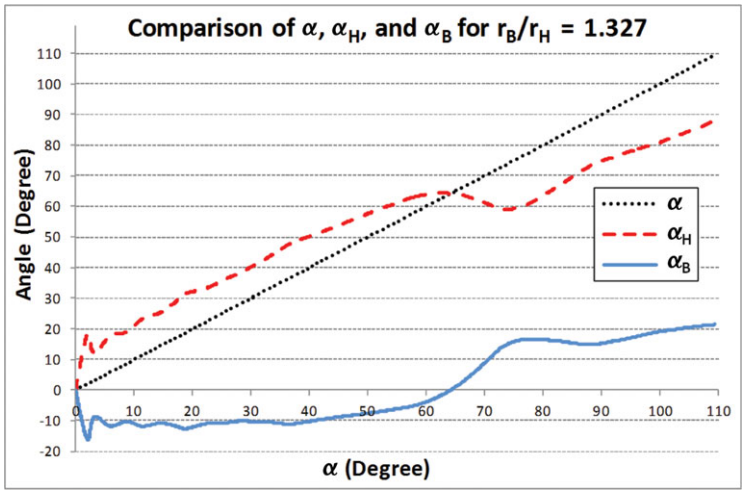


Fig. 8. (Colour online) α_H and α_B for different angles of α (r_B/r_H ratio = 1.327).

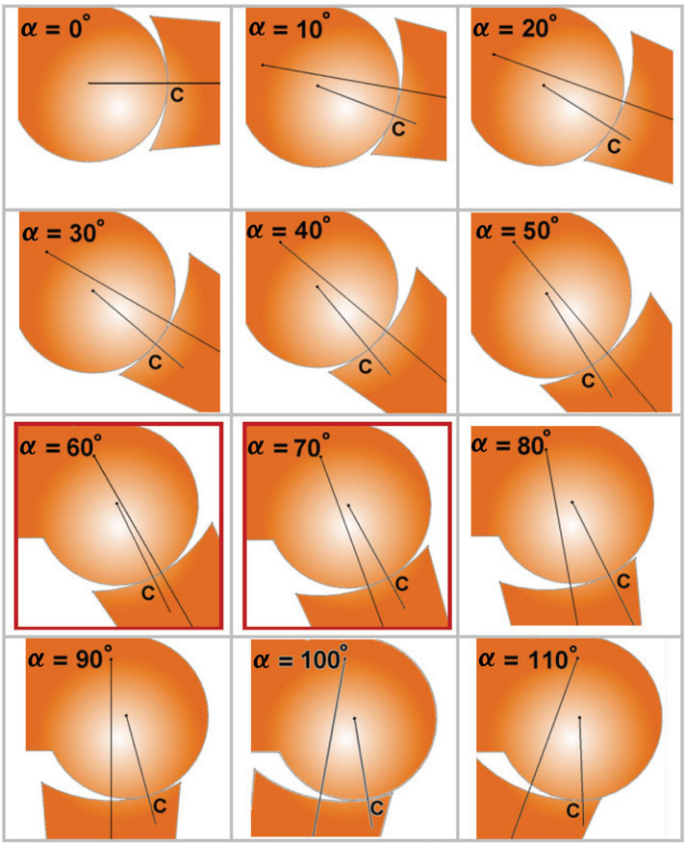


Fig. 9. (Colour online) The position of contact point C for different angles of α on two adjacent phalanges.

The values of D are shown in Fig. 10. As can be seen in this figure, the effect of "considering incongruity" or "using a hinge-like model" on the fingertip position is presented for each joint separately. Therefore, the total effect of all three joints can be calculated for different combinations of joint angles. For example, for the rotation angles of 50°, 20° and 20° of the MCP, PIP and DIP joints respectively, the distance between the fingertips in the two kinematic models is 1.41 mm whereas the maximum distance (1.71 mm) is for the rotation angles of 40°, 40° and 60°, and shows a 2% difference compared with the total length of these three phalanges.

https://doi.org/10.1017/S0263574713000817 Published online by Cambridge University Press

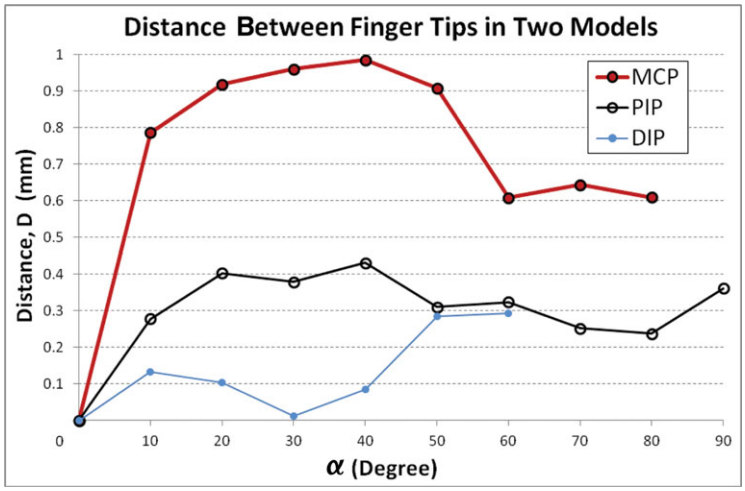


Fig. 10. (Colour online) Distance between the fingertip positions of two models when rotation only around one of the MCP, PIP or DIP joints is allowed.

Furthermore, it can be inferred from Fig. 10 that the difference of the fingertip position in the two kinematic models is a function of the joint size. This means that for bigger joints, such as knee joints, the effect of considering incongruity is more noteworthy.

4. Discussion

The data presented in Table III give a complete and real view of the behavior of human joints. At the beginning of flexion and up to a specific value of α, the values of α_B are negative when the clockwise direction is the positive direction. This means that the situation presented in Fig. 2(a) is applicable. On the contrary, these values are positive at the end of flexion, which means that the situation presented in Fig. 2(b) is applicable. Furthermore, in all the situations the relation of $\alpha = \alpha_H + \alpha_B$ remains valid.

When simulation starts, for the angles of 0°–5°, the positions of IRA are outside the range of Fig. 4 because of small vibrations of the model before it reaches a stable state. During this period, in some cases the IRA position is about 33 mm away from M_H, which can be interpreted as being located at infinity, and this means that almost a pure translation has occurred. This is an important outcome of this new model that cannot be achieved through traditional hinge-like models.

Most of the past research for the position of IRA was based on the surface marker trajectory, which determines the distance between IRA and outer surface of the finger.[18–20] Therefore, there are a few papers that indicate the position of IRA relating to the center of condyle of joints. Among these papers, Dumont[24] states that IRA lies at distance R and moves between M_H and M_B (Fig. 2). This is geometrically true and can be proved in theory if the two segments of the joints are always in contact with each other but in reality the joint segments can come apart and the model presented allows for this separation contrary to the hinge-like model. When the distance of IRA from M_H is more than R, a separation between finger segments has certainly occurred and it causes IRA to exceed the limits mentioned in refs [24, 40] by up to 33 mm.

For the r_B/r_H ratios of 1.227, 1.327 and 1.427, R is about 1.0, 1.4 and 1.7 mm respectively, and in Fig. 4, points that are not within R (1.0, 1.4 or 1.7 mm) represent a separation. In this figure the density of the locations of IRA is clearly very high, around M_H (0,0). This is in agreement with ref. [24], in which it is claimed that IRA is located closer to M_H than to M_B because the rotation around M_H is larger than the rotation around M_B.

In an experiment by Uchiyama *et al.*,[40] the locations of IRA were reported within 1 mm around M_H for normal joints, while they extended up to 2 mm following replacement of prosthetics. Here the locations of IRA are mostly within 1.5 to 2 mm around M_H depending on r_B/r_H ratio, which is quite similar to Uchiyama *et al.*'s results. It should be mentioned that in Uchiyama *et al.*'s work the measurement was performed at every 15° flexion; therefore, seven points were recorded for the

https://doi.org/10.1017/S0263574713000817 Published online by Cambridge University Press

location of IRA. Here, instantaneous measuring gives us the location of IRA as soon as it changes, therefore the results are more comprehensive.

The above-mentioned comparisons confirm the correctness of the results presented regarding the location of the axis of rotation of joints, and consequently the correct performance of the model. Therefore, the difference between fingertip positions in two models can also be reliable. However, the authors are trying to confirm this difference experimentally as a future work.

5. Conclusions

Generally in robots, in order to mimic human finger movements using the angle of its phalanges, a closed loop control is used. This closed loop control usually utilizes not only tilt sensors on robot finger but different types of sensors for measuring the position of each finger phalanx of the robot to send feedback to the control system. This helps the system to compensate errors coming from differences between the anthropometric joints (human finger joints) and the revolute joints (robot finger joints). According to the results, if an open loop control is desired to mimic human finger movements, and a precision of more than 98% for the position of the robot finger tip in comparison to the human one is desired, it is necessary to consider the incongruity of the surface curvature of finger joints. In other words, if the control system of a robot employs only the angles of human finger phalanges without any compensation of errors to mimic human finger movements, use of hinge-like joints is not acceptable for this degree of precision. Such a precision is necessary for many applications, such as touching the screen of smartphones by robot fingers or holding light and brittle objects like light bulb, in which touching of objects or applying small forces to them is desired.

Furthermore, based on the graph in Fig. 10, the effect of considering incongruity on the fingertip position is a function of joint size. This means that for bigger joints, like knee joints, this effect is more significant.

Moreover, the results show that in the finger joints, there is no constraint for the distance of IRA from the center of the condyle (M_H) and it can be between zero (when a pure rotation around M_H occurs) and infinity (when a pure translation occurs). However, IRA tends to remain within a circle with a radius of 1.5 to 2 mm around M_H, depending on r_B/r_H ratio, and almost always in quadrants II and IV of the coordinate system.

This concept and the results can be generalized for other fingers and all similar joints, such as the knee joints in sagittal plane, and can be used in humanoid robots, hand exoskeletons and robotic hands.

References

1. J. N. A. L. Leijnse and C. W. Spoor, "Reverse engineering finger extensor apparatus morphology from measured coupled interphalangeal joint angle trajectories – a generic 2D kinematic model," *J. Biomech.* **45**(3), 569–578 (2012).
2. P. Cerveri, E. D. Momi, N. Lopomo, G. Baud-Bovy, R. M. L. Barros and G. Ferrigno, "Finger kinematic modeling and real-time hand motion estimation," *Ann. Biomed. Eng.* **35**(11), 1989–2002 (2007).
3. K. S. Fok and S. M. Chou, "Development of a finger biomechanical model and its considerations," *J. Biomech.* **43**(4), 701–713 (2010).
4. D. Zhao and W. Zhang, "Topology and Analysis of Three-Phalanx COSA Finger Based on Linkages for Humanoid Robot Hands," **In**: *Proceedings of the Third International Conference on Intelligent Robotics and Applications* (*ICIRA10*), Shanghai, China (2010) 465–476.
5. L. C. Wu, G. Carbone and M. Ceccarelli, "Designing an underactuated mechanism for a 1 active DOF finger operation," *Mech. Mach. Theory*, **44**(2), 336–348 (2009).
6. G. Figliolini and M. Ceccarelli, "A novel articulated mechanism mimicking the motion of index fingers," *Robotica* **20**(1), 13–22 (2002).
7. K. Lee and J. Guo, "Kinematic and dynamic analysis of an anatomically based knee joint," *J. Biomech.* **43**(7), 1231–1236 (2010).
8. M. Mihelj, "Human arm kinematics for robot-based rehabilitation," *Robotica* **24**(03), 377–383 (2006).
9. K. S. Shih, S. C. Lin, C. K. Chao, W. S. Lee, T. W. Lu and S. M. Hou, "Biomechanical influences of pin placement and elbow angle on hinge alignment and joint distraction of bridged elbow-pin-fixator construct," *J. Biomech.* **43**(4), 757–763 (2010).
10. D. Che and W. Zhang, "GCUA humanoid robotic hand with tendon mechanisms and its upper limb," *Int. J. Soc. Robot.* **3**(4), 395–404 (2011).

https://doi.org/10.1017/S0263574713000817 Published online by Cambridge University Press

11. M. Ceccarelli, N. E. N. Rodriguez and G. Carbone, "Design and tests of a three finger hand with 1-DOF articulated fingers," *Robotica* **24**(02), 183–196 (2006).
12. M. S. Bahari, A. Jaffar, C. Y. Low, R. Jaafar, K. Roese and H. Yussof, "Design and development of a multifingered prosthetic hand," *Int. J. Soc. Robot.* **4**(1) 59–66 (2012).
13. J. U. Chu, D. H. Jeong, I. Youn, K. Choi and Y. J. Lee, "Myoelectric hand prosthesis with novel adaptive grasping and self-locking," *Int. J. Precis. Eng. Manuf.* **12**(6), 1095–1103 (2011).
14. S. Yao, M. Ceccarelli, G. Carbone, Q. Zhan and Z. Lu, "Analysis and optimal design of an underactuated finger mechanism for LARM hand," *Front. Mech. Eng.* **6**(3), 332–343 (2011).
15. J. B. Zurn, Y. Motai and S. Vento, "Self-reproduction for articulated behaviors with dual humanoid robots using on-line decision tree classification," *Robotica* **30**(2), 315–332 (2012).
16. H. S. Choi, W. Na and D. Kang, "A humanoid robot capable of carrying heavy objects," *Robotica* **29**(05), 667–681 (2011).
17. G. Carbone, *Grasping in Robotics*, *Part II, Mechanism Design* (Springer, Amsterdam, Netherlands, 2013, ISBN: 978-1-4471-4663-6), pp. 107–189. Available at: http://www.springer.com/engineering/robotics/book/978-1-4471-4663-6. Last accessed July 5, 2013.
18. J. D. Moorehead, D. M. Harvey and S. C. Montgomery, "A surface-marker imaging system to measure a moving knee's rotational axis pathway in the sagittal plane," *IEEE Trans. Biomed. Eng.* **48**(3), 384–393 (2001).
19. X. Zhang, S. W. Lee and P. Braido, "Determining finger segmental centers of rotation in flexion–extension based on surface marker measurement," *J. Biomech.* **36**(8), 1097–1102 (2003).
20. S. Koo and T. P. Andriacchi, "The knee joint center of rotation is predominantly on the lateral side during normal walking," *J. Biomech.* **41**(6), 1269–1273 (2008).
21. L. Y. Chang and N. S. Pollard, "Constrained least-squares optimization for robust estimation of center of rotation," *J. Biomech.* **40**(6), 1392–1400 (2007).
22. L. Y. Chang and N. S. Pollard, "Robust estimation of dominant axis of rotation," *J. Biomech.* **40**(12), 2707–2715 (2007).
23. S. S. H. U. Gamage and J. Lasenby, "New least squares solutions for estimating the average centre of rotation and the axis of rotation," *J. Biomech.* **35**(1), 87–93 (2012).
24. C. Dumont, G. Albus, D. Kubein-Meesenburg, J. Fanghänel, K. M. Stürmer and H. Nägerl, "Morphology of the interphalangeal joint surface and its functionaml relevance," *J. Hand Surg.* **33**(1), 9–18 (2008).
25. T. Lawrence, I. A. Trail and J. Noble, "Morphological measurements of the proximal interphalangeal joint," *J. Hand Surg.* (British and European volume) **29**(3), 242–247 (2004).
26. C. Dumont, H. Burfeind, D. Kubein-Meesenburg, N. Hosten, J. Fanghanel, T. Gredes and H. Nagerl, "Physiological functions of the human finger," *J. Physiol. Pharmacol.* **59**(Suppl 5), 69–74 (2008).
27. S. J. Leibovic and W. H. Bowers, "Anatomy of the proximal interphalangeal joint," *Hand Clin.* **10**(2), 169–178 (1994).
28. H. E. Ash and A. Unsworth, "Proximal interphalangeal joint dimensions for the design of a surface replacement prosthesis," *J. Eng. Med.* **210**(28), 95–108 (1996).
29. F. Amirouche, *Fundamentals of Multibody Dynamics. Theory and Applications* (Springer, Berlin, Germany, 2006).
30. A. A. Shabana, *Dynamics of Multibody Systems* (Cambridge University Press, Cambridge, UK, 2005).
31. I. Gibson, *Advanced Manufacturing Technology for Medical Applications: Reverse Engineering, Software Conversion and Rapid Prototyping* (John Wiley, New York, NY, 2005) pp. 123–162.
32. A. Buryanov and V. Kotiuk, "Proportions of hand segments," *Int. J. Morphol.* **28**(3), 755–758 (2010).
33. H. M. Schmidt and U. Lanz, *Surgical Anatomy of the Hand* (Thieme, Stuttgart, Germany, 2004) pp. 213–238.
34. C. Kenesi, "The interphalangeal joints of the fingers," *Anatomia Clinica* **3**, 41–48 (1981).
35. MSC Adams, *MSC Adams/View Help* (MSC Software Corporation, Santa Ana, CA, 2012).
36. D. Lindberg, "MSC Adams Modeling of Mechanical System in A400M Crew Entrance Door," *Master's Thesis* (Department of Management and Engineering, Linköping Institute of Technology, Sweden, 2012).
37. J. Engström, E. Richloow and A. Wickström, "Modeling of Robotic Hand for Dynamic Simulation," *Bachelor's Thesis* (KTH University, Stockholm, Sweden, 2010).
38. J. Giesbers, "Contact Mechanics in MSC ADAMS, a Technical Evaluation of the Contact Models in Multibody Dynamics Software MSC Adams," *Bachelor's Thesis* (Faculty of Engineering Technology, Applied Mechanics, University of Twente, Netherlands, 2012).
39. MSC Adams, "Help document for Adams/solver," Doc. ID: DOC10102, available at: http://simcompanion.mscsoftware.com/infocenter/index?page=content& id=DOC10102& cat=1VMO50& actp=LIST (2012), online. Last accessed July 2, 2013.
40. S. Uchiyama, W. P. Cooney, R. L. Linscheid, G. Niebur and K. N. An, "Kinematics of the proximal interphalangeal joint of the finger after surface replacement", *J. Hand Surg.* **25**(2), 305–312 (2000).

https://doi.org/10.1017/S0263574713000817 Published online by Cambridge University Press